4-11-2019

Comparison of TanDEM-X DEM with LiDAR Data for Accuracy Assessment in a Coastal Urban Area

Keqi Zhang

Daniel Gann

Michael S. Ross

Yuepeng Li

Jamie Rhome

remote sensing

MDPI

Article

Comparison of TanDEM-X DEM with LiDAR Data for Accuracy Assessment in a Coastal Urban Area

Keqi Zhang [1,2,*], Daniel Gann [3], Michael Ross [1,4], Himadri Biswas [1], Yuepeng Li [2] and Jamie Rhome [5]

1 Department of Earth and Environment, Florida International University, Miami, FL 33199, USA; rossm@fiu.edu (M.R.); hbisw001@fiu.edu (H.B.)
2 Extreme Events Institute, Florida International University, Miami, FL 33199, USA; yuepli@fiu.edu
3 GIS-Remote Sensing Center, Florida International University, Miami, FL 33199, USA; gannd@fiu.edu
4 Southeast Environmental Research Center, Florida International University, Miami, FL 33199, USA
5 National Hurricane Center, Storm Surge Unit, 11691 SW 17th St, Miami, FL 33165, USA; jamie.r.rhome@noaa.gov
* Correspondence: zhangk@fiu.edu; Tel.:+1-305-348-1607

Received: 4 March 2019; Accepted: 1 April 2019; Published: 11 April 2019

Abstract: The TanDEM-X (TDX) mission launched by the German Aerospace Center delivers unprecedented global coverage of a high-quality digital elevation model (DEM) with a pixel spacing of 12 m. To examine the relationships of terrain, vegetation, and building elevations with hydrologic, geologic, geomorphologic, or ecologic factors, quantification of TDX DEM errors at a local scale is necessary. We estimated the errors of TDX data for open ground, forested, and built areas in a coastal urban environment by comparing the TDX DEM with LiDAR data for the same areas, using a series of error measures including root mean square error (RMSE) and absolute deviation at the 90% quantile (LE90). RMSE and LE90 values were 0.49 m and 0.79 m, respectively, for open ground. These values, which are much lower than the 10 m LE90 specified for the TDX DEM, highlight the promise of TDX DEM data for mapping hydrologic and geomorphic features in coastal areas. The RMSE/LE90 values for mangrove forest, tropical hardwood hammock forest, pine forest, dense residential, sparse residential, and downtown areas were 1.15/1.75, 2.28/3.37, 3.16/5.00, 1.89/2.90, 2.62/4.29 and 35.70/51.67 m, respectively. Regression analysis indicated that variation in canopy height of densely forested mangrove and hardwood hammock was well represented by the TDX DEM. Thus, TDX DEM data can be used to estimate tree height in densely vegetated forest on nearly flat topography next to the shoreline. TDX DEM errors for pine forest and residential areas were larger because of multiple reflection and shadow effects. Furthermore, the TDX DEM failed to capture the many high-rise buildings in downtown, resulting in the lowest accuracy among the different land cover types. Therefore, caution should be exercised in using TDX DEM data to reconstruct building models in a highly developed metropolitan area with many tall buildings separated by narrow open spaces.

Keywords: TDX; LiDAR; DTM; DSM; horizontal accuracy; vertical accuracy; error measures

1. Introduction

Digital terrain and surface models (DTM and DSM) are essential for modeling freshwater and coastal flooding, estimating vegetation biomass and carbon storage, monitoring urban changes, and quantifying the effects of human activity on climate [1–3]. Airborne light detection and ranging (LiDAR), an active remote sensing technology, provides accurate and high-resolution measurements of topography, vegetation, and buildings on the Earth's surface [4]. During the past twenty years,

airborne LiDAR mapping has gradually become the preferred means to derive DTM and DSM in developed countries. However, the cost of data collection and processing prohibits the extensive utilization of LiDAR technology in the developing world, and even in large developed countries for nationwide mapping. In addition, changes in vegetation, buildings, and topography caused by human activity occur on a global scale, thus global DTM and DSM are needed to assess the cumulative effect of human-induced changes on climate and disasters such as flooding. Satellite based technology like synthetic aperture radar (SAR), which is independent of sunlight, cloud, and weather, offers a viable option for collecting global elevations of the Earth's surface [5].

In 2000, the shuttle radar topography mission (SRTM) created a digital elevation model (DEM) for lands between latitude 60°N and 56°S [6], and provided the first free global topographic data set for large-scale hydrological process studies [7]. Note that the term DEM, representing the elevations from a datum to the tops of vegetative, built, or ground surfaces, is often used as the generic term for DSM and DTM by many data providers [8]. Unfortunately, the coarse pixel spacing (30 m at best) and large vertical error (5.6–9.0 m at the 90% quantile) [9] limits the application of SRTM DEMs in hydrologic and geomorphic studies in low-relief areas, although vertical error in such settings is at the low end of the distribution [10,11]. Additionally, ground elevation in densely vegetated and built floodplains is often overestimated because the SRTM sensor detects a surface midway between the bare ground and the canopy. It is challenging to remove vegetation and buildings from SRTM DEMs to derive DTM because of the coarse horizontal (30 m) and vertical (1 m) resolutions. In order to fill the gap in high quality global DTM and DSM data for many applications associated with ecology, geology, geomorphology and hydrology, the German Aerospace Center (DLR), in partnership with private industry, launched the TanDEM-X (TDX) DEM mission from 2010 to 2015 [12–14]. By employing bistatic X-band SAR sensors mounted on two closely flying satellites, the TDX DEM mission achieved an absolute vertical error of 10 m at the 90% quantile (LE90) and a relative vertical error of 2–8 m at an approximate pixel spacing of 12 m. The vertical errors of TDX DEMs have been determined by comparing the data with GPS control points, ice, cloud, and land elevation satellite (ICESat) LiDAR measurements, and SRTM DEMs on the continental level [12,15–17]. The TDX DEM dataset provides a consistent and global source for estimating the elevations of terrain, vegetation, and buildings by covering all of the Earth's surface at least twice during the mission [12,18].

In 2014, the DLR released the intermediate TDX DEM (IDEM) data to the scientific community for experimental research, based on the first-pass of the TDX DEM mission [19]. The IDEMs were subsequently verified by ICESat, airborne LiDAR and GPS measurements at many study sites [20–23] and have been used to map canopy heights of boreal forests [24], urban tree heights [25], and building heights [26]. In 2016, the DLR released the final TDX DEM product to the scientific community [27]. The accuracy of the final TXD DEM was improved by inclusion of measurements from multiple flight paths and quality control. Rizzoli et al. [12] and Wessel et al. [17] conducted vertical accuracy assessment by comparing TDX DEM elevation with ICESat, GPS and LiDAR height measurements on a global scale and demonstrated that the LE90 error of the TDX DEM in areas not covered by ice or forest was only 0.88 m, much lower than the LE90 value specified for the product and highlighting the potential of TDX DEMs for many applications requiring elevations of terrain, trees, and buildings. However, the categories of land cover on which the global accuracy analysis was conducted were too generic and the question whether and how the vertical accuracy of the final TDX DEM product varies as land cover types change remained to be answered. In addition, the horizontal accuracy of TDX DEMs, which is important to analyze the geometric characteristics of Earth's surface features has not been examined. Therefore, to provide guidance for users to appropriately utilize the data for mapping terrain elevations, canopy heights, above ground biomass, and building heights, the accuracy of final TDX DEMs must be examined systematically for detailed types of land cover at a local scale. The landscape of south Florida, USA, which includes a mixture of high-rise buildings, single-family residential homes, condominiums, and trees as well as surrounding preserved forests and wetlands within Everglades National Park, is an ideal location for examining the accuracy of the final TDX

DEM products. The objective of this paper is to estimate the accuracy of TDX DEM data in urban, wildland and wetland environments by comparing TDX DEMs with airborne LiDAR measurements. More specific objectives include (1) quantifying the horizontal and vertical errors of TDX DEMs in open ground without buildings and trees, (2) estimating the vertical errors of TDX canopy heights in subtropical and tropical slash pine, hardwood hammock, and mangrove forests, and (3) assessing the vertical accuracy of TDX building measurements in high-rise and single-family residential areas.

2. Materials and Methods

2.1. The Study Area

The study area is Miami-Dade County in South Florida, USA, where high resolution LiDAR data were collected in 2015. Miami-Dade County is bounded by Biscayne Bay and the Atlantic Ocean on the east, Florida Bay on the south, Everglades National Park to the west, and Broward County on the north (Figure 1a). The earliest urban development occurred in the eastern portion of the county, following the Atlantic Coastal Ridge, where elevations reach 4–6 m above the current sea level [28]. Subsequently, and especially in the past 30 years, the built area expanded toward the Everglades, the largest subtropical wetland in North America. High-rise buildings are clustered downtown in the northeastern part of the County next to Biscayne Bay, while single-family and condominium residential areas surrounding the urban core occupy the greatest portion of the area. Large tracts of agricultural land prevail in the less developed southwest, shore-parallel bands of mangrove forest occur along the southeastern and southern coasts, and small tracts of pine and hardwood hammock (i.e., mesic broadleaved forests with trees of tropical origin) occupy an area inside Everglades National Park. With a gently sloped topography and vast areas only a few meters above the current sea level, Miami-Dade County is one of the most vulnerable areas in the USA to storm surge, sea level rise, and urban freshwater flooding (Figure 1b). The total population, real property, and gross domestic product of Miami-Dade County represent about 15% of the total for the State of Florida which is composed of 67 counties [29], making Miami-Dade one of Florida's social and economic centers.

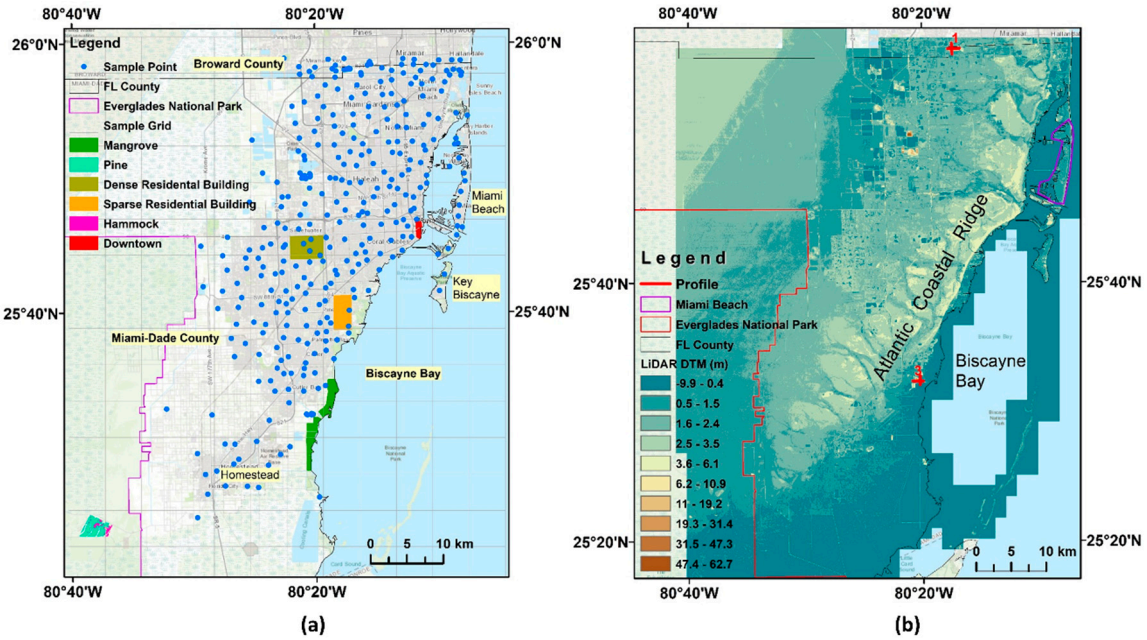

Figure 1. (**a**) The study site and locations of sample grids and sample points for open ground; (**b**) the LiDAR DTM of Miami-Dade County and the locations of profiles at two trash mounds for examining the horizontal accuracy of TDX DEMs.

2.2. Data

The 1° × 1° (N25°W081°) TDX DEM tile that was collected in 2013 and 2014 covers urban Miami-Dade County and part of the Everglades. The pixel spacing of the TDX DEM is 0.4 arc seconds (about 12 m) in latitudinal direction, and varies in longitudinal direction between 0.4 arc seconds at the equator and 4 arc seconds above 85°N/S latitude [13]. The TDX twin X-band SAR sensors in a bistatic mode utilize the strip-map mode with a resolution of 3 m, swath width of 30 km, and slant angles of 30°–50° to derive the elevations of the Earth's surface [3,30]. The 32 bit float elevations of the TDX DEM were generated by averaging all SAR height values falling in a given pixel using weights based on the standard deviations of the errors for these heights. For each DEM image, there are seven auxiliary information layers including height error map (HEM), SAR mean amplitude mosaic (AMP), SAR minimum amplitude mosaic (AM2), water indication mask (WAM), coverage map (COV), consistency mask (COM), and layover and shadow mask (LSM). The horizontal datum for DEM and auxiliary images is WGS84-G1150 and the heights of the DEM are ellipsoid heights referenced to WGS84-G1150 [31]. It is noteworthy that the TDX DEMs represent DSMs including canopy and building measurements because electronic and magnetic waves emitted and recorded by radar cannot penetrate fully through vegetation and buildings to reach the ground.

Airborne LiDAR data were acquired using a Rigel LMS-Q680i scanner mounted on a Cessna 206 flying at an altitude of 550 m with a moving speed of 57 m/s. The laser scanner ranged the Earth's surface at a pulse rate of 400 KH and a 60 degree field of view, resulting in a point density of 8 points per square meter [32]. Most of the 4,175 km^2 surveyed area was covered by east-west oriented and 50% overlapped swaths collected in February and April 2015. The LiDAR points in binary LAS (https://www.asprs.org/divisions-committees/lidar-division/laser-las-file-format-exchange-activities, accessed 27 January 2019) format and a 1.5 m (5 ft) bare earth DTM were delivered to Miami-Dade County by the vendor in state plane projection (feet) with high accuracy reference Network (HARN) North American Datum of 1983 (NAD83) and the vertical North American Datum of 1988 (NAVD88). The vertical root mean square error (RMSE) of the LiDAR data was about 0.06 m, based on comparison of LiDAR DTM with 97 GPS measurements at well-defined road surfaces, and horizontal RMSE was less than 0.067 m.

Auxiliary data used in the analysis include GPS survey benchmark data in the City of Miami Beach, a land use map created by South Florida Water Management District (SFWMD) in 2009 [33], a vegetation map for the Everglades National Park created by the University of Georgia (UG) in 1998 [34], and an urban land cover map for Miami-Dade County created by University of Florida and Florida International University (UF-FIU) in 2016 [35]. The SFWMD land use map was generated by photo-interpretation of 2008–2009 aerial photography, using the Florida Land Use and Cover Classification System [36] modified by SFWMD. The SFWMD map covers the urban and agricultural areas of Miami-Dade County with minimum mapping units of 0.8 hectares for wetlands and two hectares for uplands, but does not cover most forest areas in Everglades National Park. The UG map, with a minimum mapping unit of one hectare, was created by digitizing color-infrared aerial photographs of 1:40,000 scale obtained in 1994 and 1995, and covers all of the Everglades National Park.

The UF-FIU land cover map was generated for the urban area of Miami-Dade County using WorldView-2 images with a 2 m pixel spacing acquired between 2011 and 2014 [35]. Atmospherically corrected multi-spectral images were initially classified using a random forest algorithm. Various vector data layers provided by Miami-Dade County were incorporated into the map generation process to improve the accuracy of the initial classification; these included large buildings, small buildings, pavement edges, railroads, water bodies, and agricultural areas. The classification accuracy was estimated to be 90% with a 95% confidence based on a stratified random sampling method. The UF-FIU land cover product had varying minimum mapping units for different categories, ranging from 8 m^2 for trees and buildings to 200 m^2 for wetland and cropland. Due to its higher spatial resolution, the UF-FIU land cover data were used for the entire area covered by the UF-FIU map, and the SFWMD and UG maps were used in the remaining areas.

2.3. Datum Conversion

In order to make a consistent comparison among TDX and LiDAR DEMs, all measurements must refer to the same horizontal and vertical datum. Hence, all data were converted to State Plan HARN NAD83 horizontal datum and NAVD88 vertical datum in units of meters using the National Geospatial-Intelligence Agency (NGA) Conversion Tool (http://earth-info.nga.mil/GandG/wgs84/gravitymod/egm96/egm96.html, accessed 27 January 2019), National Oceanic and Atmospheric Administration (NOAA) VDatum (https://vdatum.noaa.gov/, accessed 27 January 2019), and the ArcGIS Projection tool following the flowchart in Figure 2. For LiDAR data, the 5 ft LiDAR DTM was first converted to a 1.5 m LiDAR DTM in the State Plane meter coordinate system in ArcGIS using the Raster Projection tool with the nearest neighbor resampling method and the Map Algebra tool. Then a 12 m DTM was generated by averaging the 1.5 m LiDAR DTM using the Raster Aggregation tool in ArcGIS. The 12 m DSM was generated following a similar procedure. First, a 5 ft DSM was generated from the first return measurements of the LAS point data in ArcGIS using the Mosaic Dataset tool. Then, the 5ft DSM was converted to 1.5 m DSM in the State Plane and NAVD 88 coordinate system and aggregated to 12 m. For TDX data, the DEM was first converted to an ASCII text file using the Raster to ASCII tool in ArcGIS. Then, the elevations in the ASCII file were converted to State Plane HARN NAD 83 (meter) elevations with NAVD88 vertical datum using the VDatum tool. The GEOID12A model was used when ellipsoid heights were converted to NAVD88 because the LiDAR measurements were converted to NAVD88 from ellipsoid heights using GEOID12A [32]. Finally, the ASCII file with converted elevations was transferred back to an image file using the ASCII to Raster tool in ArcGIS. The entire transformation procedure was automated using Python script. The auxiliary GPS survey benchmark data, SFWMD land use map, UG vegetation map, and UF-FIU urban land cover map were all converted to the same reference system in ArcGIS.

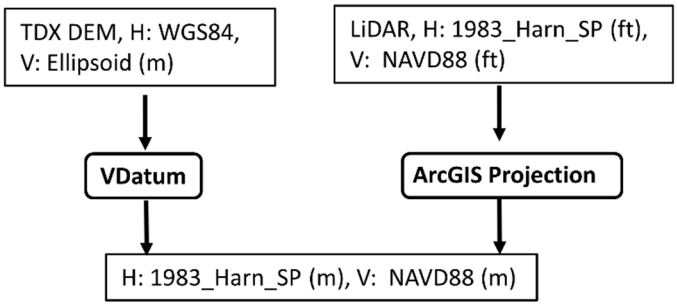

Figure 2. Flowchart for datum conversion.

2.4. Accuracy Analysis

A collection of 210 survey benchmarks in the City of Miami Beach were employed to examine the accuracy of the 1.5 m LiDAR DTM. Survey benchmarks on bridges and other non-ground features, and within 10 m of the shoreline were removed, retaining 152 survey benchmarks used in the analysis. LiDAR DTM cells close to the shoreline have relatively large vertical errors because the filtering method to separate ground and non-ground points often performs poorly here due to the influence of the water body and missing data, and the horizontal error has a large impact on vertical accuracy due to a relatively steep slope between the land and water surface. The elevations of grid cells of the 1.5 m LiDAR DTM in which the benchmarks fall were extracted using the extract point tool in ArcGIS to make the comparison between LiDAR DTM and survey benchmark elevations.

The accuracy of TDX DEM was analyzed for the selected land cover types in Miami-Dade County by comparing it with the 12 m LiDAR DSM. Since the LiDAR data and TDX DEM were not collected simultaneously, cover types such as agricultural land that might change substantially between 2013 and 2015 were not included in the analysis. Water bodies were also excluded from the accuracy analysis because of low backscatter of LiDAR and SAR beams on smooth water surfaces [4,37]. High-rise

buildings, low-rise commercial and residential buildings, and wooded areas for which little change was expected over the period were selected for analysis. Open spaces such as sports fields, golf courses, lawns, and landfills of sufficient size to expect consistent ground elevations were selected to determine the TDX DEM errors for open ground (terrain). A systematic sampling method was employed to select the check points (pixels) for open ground by dividing the study area into square tiles. Since the locations of sample pixels were often limited by the number and spatial distribution of open spaces within a tile, it was impractical to attain a perfectly even distribution of samples. To select check points in a consistent manner, the study area was first divided into 5 × 5 km tiles, and then the pixels were visually sampled as evenly as possible within each tile. An auxiliary criterion was to choose pixels whose elevations were similar to those of neighboring pixels, in order to maximize the representativeness of the sample, and reduce the effect of possible horizontal errors of the TDX data (Figure 3).

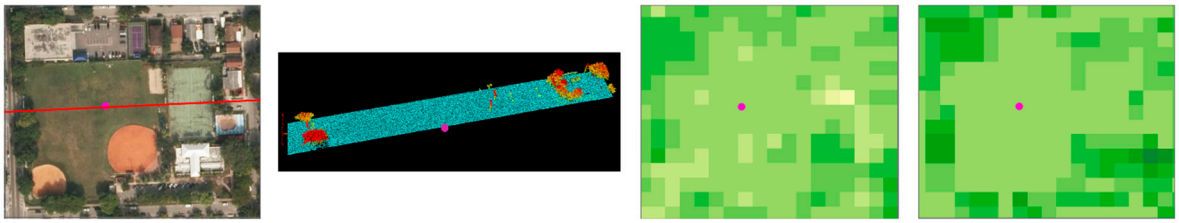

Figure 3. (**a**) Aerial photograph, (**b**) LiDAR points, (**c**) TDX DEM, and (**d**) LiDAR DSM for an open ground sample site. Both TDX DEM and LiDAR DSM have a horizontal resolution of 12 m.

Comparison of the TDX DEM and LiDAR DSM elevation differences of open ground free from the influence of non-ground features is relatively straightforward. However, analysis of TDX DEM and LiDAR DSM elevation differences in areas with buildings and trees is more complex because the interaction of the radar beams from the TDX satellites with both ground and non-ground features influence SAR elevation measurements [1]. To examine the effect of buildings and trees on TDX elevation measurements, sample areas covering dense tall buildings in the urban core, sparse residential buildings surrounded by dense trees, dense residential buildings with sparse trees, and forests including mangrove, hardwood hammock, and slash pine (*Pinus elliottii var densa*) woodlands were selected to analyze the differences between TDX DEM and LiDAR DSM across units recognized in land cover and use maps.

Given a test DEM (TDX DEM) elevation (y_i) and reference (LiDAR DSM) elevation (x_i) at sample point i, the difference (Δh_i) between y_i and x_i, and the total number of samples (N), the following metrics were employed to quantify the vertical errors of DEMs [17,38–40]:

$$\textit{Mean Error}: \quad ME = \frac{1}{N}\sum_{i=1}^{N}(y_i - x_i) = \frac{1}{N}\sum_{i=1}^{N}\Delta h_i \tag{1}$$

$$\textit{Absolute Mean Error}: \quad AME = \frac{1}{N}\sum_{i=1}^{N}|\Delta h_i| \tag{2}$$

$$\textit{Mean Normalized Bias}: \quad MNB = \frac{1}{N}\sum_{i=1}^{N}\frac{\Delta h_i}{x_i}\cdot 100\% \tag{3}$$

$$\textit{Root Mean Square Error}: \quad RMSE = \sqrt{\frac{1}{N}\sum_{i=1}^{N}\Delta h_i^2} \tag{4}$$

$$\textit{Standard Deviation}: \quad SD = \sqrt{\frac{1}{N-1}\sum_{i=1}^{N}(\Delta h_i - ME)^2} \tag{5}$$

These error measures perform well if the Δh_i follows a normal distribution, however, the error distribution of a DEM is often not normal [39,40]. Therefore, Höhle and Höhle [39] proposed the following robust accuracy measures based on non-parametric statistics for vertical DEM errors that do not follow normal distributions:

$$\textit{Median (50\% quantile) of Differences}: \quad MD = Q_{\Delta h}(0.5) = m_{\Delta h} \tag{6}$$

$$\textit{Normalized Median Absolute Deviation}: \quad NMAD = c{\cdot}median(|\Delta h_i - m_{\Delta h}|) \tag{7}$$

$$\textit{Absolute Deviation at 90\% Quantile}: \quad LE90 = Q_{|\Delta h|}(0.9) \tag{8}$$

The constant c in Equation (7) is approximately equal to 1.4826 (which is the value used in this paper) if the distribution of Δh_i is normal after disregarding the abnormality induced by outliers [41,42]. NMAD is a more robust estimator for the deviation of non-normally distributed data that have outliers. The absolute deviations at the 68.3% and 95% quantiles were employed by Höhle and Höhle [39] and Müller et al. [40] to specify the elevation error range, while LE90 (Equation (8)) was used by Wessel et al. [17] to align the error calculation to the accuracy specification of TDX DEM [14]. We followed the latter procedure and represented the deviation by LE90.

Linear regression was also utilized to examine the correlation between LiDAR and TDX DEM elevations

$$y_i = a + bx_i + \varepsilon_i \tag{9}$$

The variable ε_i is the random error following a normal distribution. The R-squared value of the linear regression equation was calculated by

$$R^2 = \frac{\sum_{i=1}^{N}(a + bx_i - y_m)^2}{\sum_{i=1}^{N}(y_i - y_m)^2} \tag{10}$$

The variable y_m is the mean of y_i. The p-value (i.e., the two-sided probability value for a null hypothesis that the slope of the regression equation is zero [38]) was employed to examine the significance of the regression parameter. A low p-value (e.g., < 0.01) indicates that the null hypothesis should be rejected.

Examination of TDX DEM's horizontal accuracy is more challenging than its vertical accuracy because of the difficulty in finding reference features. Two landfills located at the north and south ends of the study area were selected for comparison analysis (Figure 1b). The surface and neighborhood of the two trash mounds were free from trees and tall buildings, minimizing errors of multipath reflection and shadow effect from SAR. Sample points at a spacing of 12 m along two perpendicular transects were extracted from TDX DEM and LiDAR DSM for error analysis. A spatial correlation analysis [38] was employed to analyze possible shifts in the TDX DEM:

$$r_k = \frac{1}{N-k}\sum_{i=1}^{N-k}\left(\frac{x_i - x_m}{s_x}\right)\cdot\left(\frac{y_{i+k} - y_m}{s_y}\right) \tag{11}$$

The variable x_i is the LiDAR DSM elevation at sample point i, and y_{i+k} is the TDX DEM elevation at sample point i+k. The variables x_m, y_m, s_x, and s_y are means and standard deviations of x_i and y_i, The index k is the spatial lag between sample points x_i and y_{i+k} with a maximum value of $N/2$.

3. Results

3.1. LiDAR DTM Accuracy and Horizontal Accuracy of TDX DEM

The vertical RMSE of the 1.5 m LiDAR DTM was about 0.10 m (Figure 4), indicating that the vendor's vertical accuracy claim (RMSE = 0.06) for the urban area was reasonable given that a considerable number of benchmarks were located at the edges of street curbs, which were usually 0.15 m higher than the adjacent road surface. The DTM value at these benchmarks was generated by interpolating the points at the higher curb and lower road surface. Also, there was no large systematic offset between LiDAR DTM and GPS measurements as indicated by a low intercept value of 0.05 m in the linear equation. It should be noted that these GPS benchmarks are only available in urban settings with commercial buildings, residential homes, open ground, and forested parks, which do not represent all land cover types in the study area. It is expected that the vertical accuracy of LiDAR DTMs vary in the forested and marsh areas, depending upon the coverage of trees, low vegetation, and ground [1].

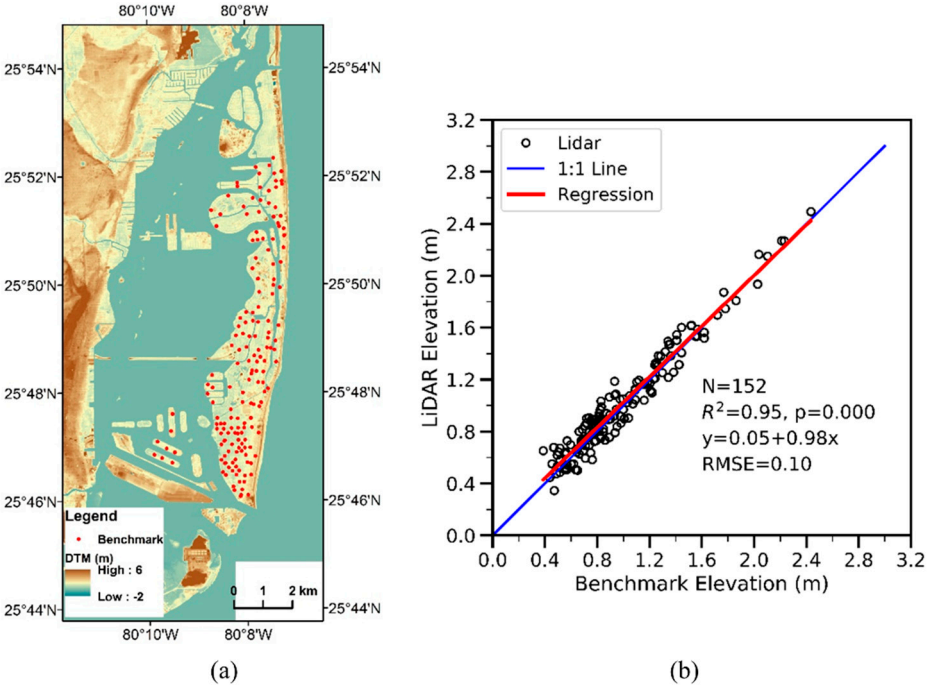

Figure 4. (**a**) The GPS benchmarks in the City of Miami Beach and (**b**) the linear regression between GPS benchmark and LiDAR DTM elevations.

LiDAR DSM and TDX DEM elevations along four transects across two trash mounds were analyzed to detect the magnitude of the horizontal shift in TDX DEM (Figure 5). The TDX DEM elevations matched well with the LiDAR DSM elevations in most cases along four profiles, although there were considerable differences at several locations along Profiles 2 and 3. The correlation analysis between TDX DEM and LiDAR DSM indicated that the correlation coefficients with a lag value of 0 reached maxima with r values of 0.99, 0.88, 0.99, and 0.97, respectively, for Profiles 1, 2, 3, and 4. The relatively low correlation coefficient of Profile 2 was caused by the large fluctuation of TDX DEM elevations over a water surface that occupied the interval between 100 m and 400 m (Figure 5). The correlation coefficient with 0 lag for Profile 2 reached 0.99 if the elevations less than 400 m were removed from the calculation. Thus, the spatial correlation analysis demonstrated that there was no significant horizontal shift in TDX DEM.

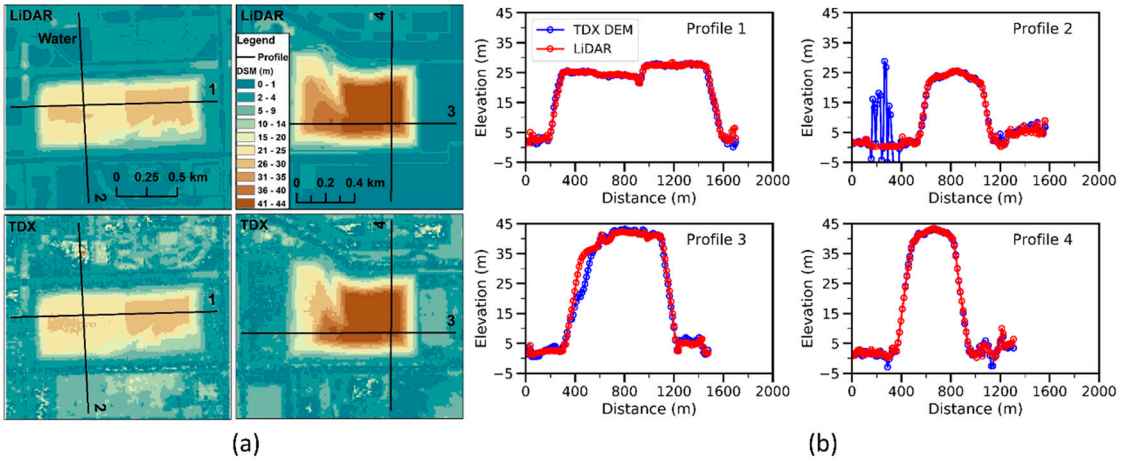

Figure 5. (**a**) TDX DEM of 12 m pixel size and corresponding LiDAR DSM of two trash mounds for profile analysis. Note that the TDX DEM image shows more noise than LiDAR DSM, especially in water bodies. (**b**) Elevation profiles extracted from TDX DEM and LiDAR DSM for two trash mounds.

3.2. *Vertical Accuracy for Different Types of Land Cover*

The RMSE and LE90 values of TDX DEM elevations versus LiDAR DSM elevations for the land area of 3500 km^2 were 2.25 m and 2.30 m (Table 1), respectively. The RMSE value was reduced to 1.80 m if pixels with height errors larger than 1 m in the corresponding HEM map were removed, while the RMSE value became 1.81 m after removing large height inconsistent pixels by selecting only pixels with COM values of 2, 8, and 10. These numbers represented smaller inconsistency (2), all height consistency (8), and smaller inconsistency but at least one consistent height pair (10) in SAR measurements [13]. The RMSE value was reduced to 1.67 m if both criteria were used to select the pixels. The linear regression between TDX DEM and LiDAR DSM elevations showed that the correlation was highest when both criteria were used to select pixels, generating an *R*-squared value of 0.68. The analysis of errors revealed the overall accuracy of TDX DEM elevations for the entire study area that was occupied by various types of land cover. The interaction between incident radar waves with different objects on the Earth's surface varied with land cover type, resulting in the fluctuation of SAR measurement uncertainty. Additionally, agricultural land which may have changed in the period between TDX DEM mission and LiDAR surveys were not excluded from the error analysis for the entire study area. Therefore, it was necessary to conduct an error analysis of TDX DEM for individual types of land cover expected to undergo minimal temporal change as shown in the following sections.

3.2.1. Open Ground Area

Figure 6 shows an almost perfect one to one relationship between the LiDAR DSM and LiDAR DTM elevations for open ground areas. Based on the linear regression between these two values, DTM values were only 0.02 m lower than DSM values. This was expected because there were few above ground features in open ground locations. The TDX DEM elevations were lower than LiDAR DSM elevations by 0.13 m in terms of the median of the elevation difference values (Table 1). The histograms in Figure 7a,b illustrate that open ground differences exhibited the least variation of all land cover types, and most differences were within the range of −2.0 m to +1.5 m. The RMSE and LE90 errors of TDX DEM elevations versus LiDAR DSM elevations were 0.49 m and 0.79 m, respectively, for 326 sample locations (Table 1). The RMSE and LE90 values were reduced to 0.48 m and 0.78 m if pixels with height errors greater than 1 m were removed, while these values increased to 0.49 m and 0.80 m after removing large height-inconsistent pixels (COM values other than 2, 8, and 10). The RMSE and LE90 values were reduced to 0.48 m and 0.78 m again if both criteria were used to select the pixels. In contrast to a small variation of RMSE values, the NMAD values had the same value of 0.41 m for the four pixel selection criteria (Table 1). The reason for small changes of RMSE and NMAD was that only a few pixels had large height errors and/or height inconsistency. The linear regression between TDX

DEM and LiDAR DSM elevations showed that they too had an almost one-to-one relationship, with a small intercept value of −0.16 m and coefficient of 1.01 (Figure 6). These demonstrated that the TDX DEM vertical accuracy for open ground was much smaller than the error range of 10 m specified by product guidance [13].

Table 1. Error measures and linear regression parameters for TDX DEM versus LiDAR elevations. Case 1 (e.g., P-1) is for all pixels in a sample area. Case 2 (e.g., P-2) is for the pixels after the removal of height errors larger than 1 m in terms of the corresponding HEM map for the TDX DEM. Case 3 (e.g., P-3) is for the pixels after the removal of large height inconsistent pixels by selecting the pixels with COM values of 2, 8, and 10. Case 4 (e.g., P-4) is for the pixels after the removal of the pixels by applying both criteria. LC: Land Cover; NP: Number of Pixels; PC: Percentage calculated by (number of all pixels - number of pixels after removal of inconsistent pixels)/number of all pixels × 100; PV: *P*-Value; EA: Entire Area; OG: Open Ground; M: Mangrove; H: Hammock; P: Pine; D: Downtown; SR: Sparse Residential areas, DR: Dense Residential areas. The definition of ME, MD, AME, MNB, SD, RMSE, NMAD, LE90, and R^2 can be found in Equations (1)–(10).

LC	NP/PC	ME	MD	AME	MNB	SD	RMSE	NMAD	LE90	R^2	PV
EA-1	24671844/0	−0.51	0.42	0.94	2.8	2.19	2.25	0.62	2.30	0.52	0.000
EA-2	24284337/1.6	−0.50	0.41	0.89	2.9	1.73	1.80	0.61	2.23	0.65	0.000
EA-3	24362012/1.3	−0.49	0.41	0.90	2.8	1.74	1.81	0.61	2.26	0.64	0.000
EA-4	24057905/2.5	−0.49	0.40	0.88	2.9	1.60	1.67	0.60	2.21	0.68	0.000
OG-1	326/0	−0.15	−0.13	0.37	−7.3	0.47	0.49	0.41	0.79	0.99	0.000
OG-2	319/2.1	−0.14	−0.13	0.36	−6.5	0.46	0.48	0.41	0.78	0.99	0.000
OG-3	325/0.3	−0.15	−0.13	0.37	−7.3	0.47	0.49	0.41	0.80	0.99	0.000
OG-4	319/2.1	−0.14	−0.13	0.36	−6.5	0.46	0.48	0.41	0.78	0.99	0.000
M-1	94040/0	−0.65	−0.46	0.77	−21.1	0.95	1.15	0.60	1.75	0.95	0.000
M-2	93026/1.1	−0.64	−0.45	0.76	−21.4	0.91	1.11	0.59	1.70	0.95	0.000
M-3	93621/0.4	−0.65	−0.46	0.77	−21.3	0.93	1.13	0.60	1.73	0.95	0.000
M-4	92752/1.4	−0.64	−0.45	0.75	−21.6	0.90	1.10	0.59	1.69	0.95	0.000
H-1	7943/0	−1.97	−1.93	2.01	−23.2	1.15	2.28	1.00	3.37	0.86	0.000
H-2	7936/0.1	−1.97	−1.93	2.01	−23.2	1.15	2.28	1.00	3.37	0.86	0.000
H-3	7943/0	−1.97	−1.93	2.01	−23.2	1.15	2.28	1.00	3.37	0.86	0.000
H-4	7936/0.1	−1.97	−1.93	2.01	−23.2	1.15	2.28	1.00	3.37	0.86	0.000
P-1	42253/0	−2.60	−2.35	2.64	−46.0	1.80	3.16	1.66	5.00	0.14	0.000
P-2	38943/7.8	−2.55	−2.30	2.58	−46.0	1.73	3.08	1.60	4.85	0.16	0.000
P-3	42253/0	−2.65	−2.35	2.64	−46.0	1.80	3.16	1.66	5.00	0.14	0.000
P-4	38943/7.8	−2.55	−2.30	2.58	−46.0	1.73	3.08	1.60	4.85	0.16	0.000
D-1	12146/0	−14.35	−2.42	18.03	−36.9	32.70	35.70	7.99	51.67	0.00	0.000
D-2	6860/43.5	−9.23	−1.50	11.85	−10.2	25.23	26.86	4.94	33.73	0.01	0.000
D-3	6921/43.0	−8.48	−1.20	10.91	−2.4	24.93	26.33	4.55	29.10	0.01	0.000
D-4	5172/57.4	−7.20	−1.13	9.19	−4.6	22.35	23.48	3.82	22.49	0.00	0.000
SR-1	79565/0	−0.86	−0.70	2.01	−1.5	2.48	2.62	2.31	4.29	0.44	0.000
SR-2	79526/0.0	−0.86	−0.70	2.01	−1.5	2.48	2.62	2.31	4.28	0.44	0.000
SR-3	79523/0.1	−0.86	−0.70	2.01	−1.5	2.48	2.62	2.31	4.29	0.44	0.000
SR-4	79491/0.1	−0.86	−0.70	2.01	−1.5	2.48	2.62	2.31	4.28	0.44	0.000
DR-1	100253/0	−0.75	−0.62	1.37	−9.1	1.74	1.89	1.42	2.90	0.23	0.000
DR-2	99687/0.6	−0.76	−0.62	1.37	−9.1	1.73	1.89	1.42	2.89	0.23	0.000
DR-3	100005/0.2	−0.75	−0.62	1.37	−9.1	1.73	1.89	1.42	2.89	0.23	0.000
DR-4	99472/0.8	−0.75	−0.62	1.37	−9.1	1.73	1.88	1.42	2.89	0.23	0.000

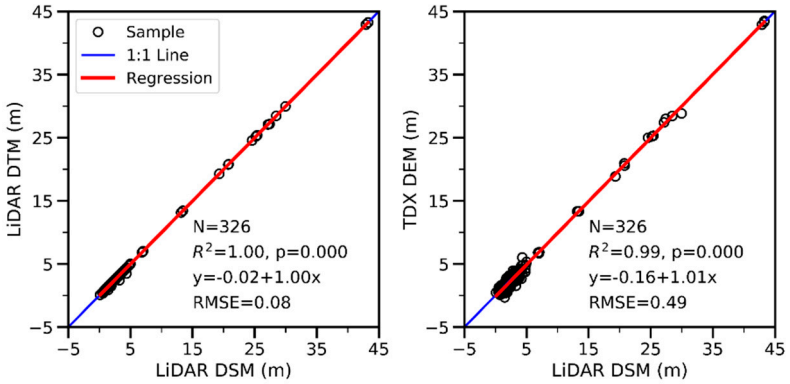

Figure 6. From left to right, linear regressions of LiDAR DTM versus LiDAR DSM elevations and TDX DEM versus LiDAR DSM elevations.

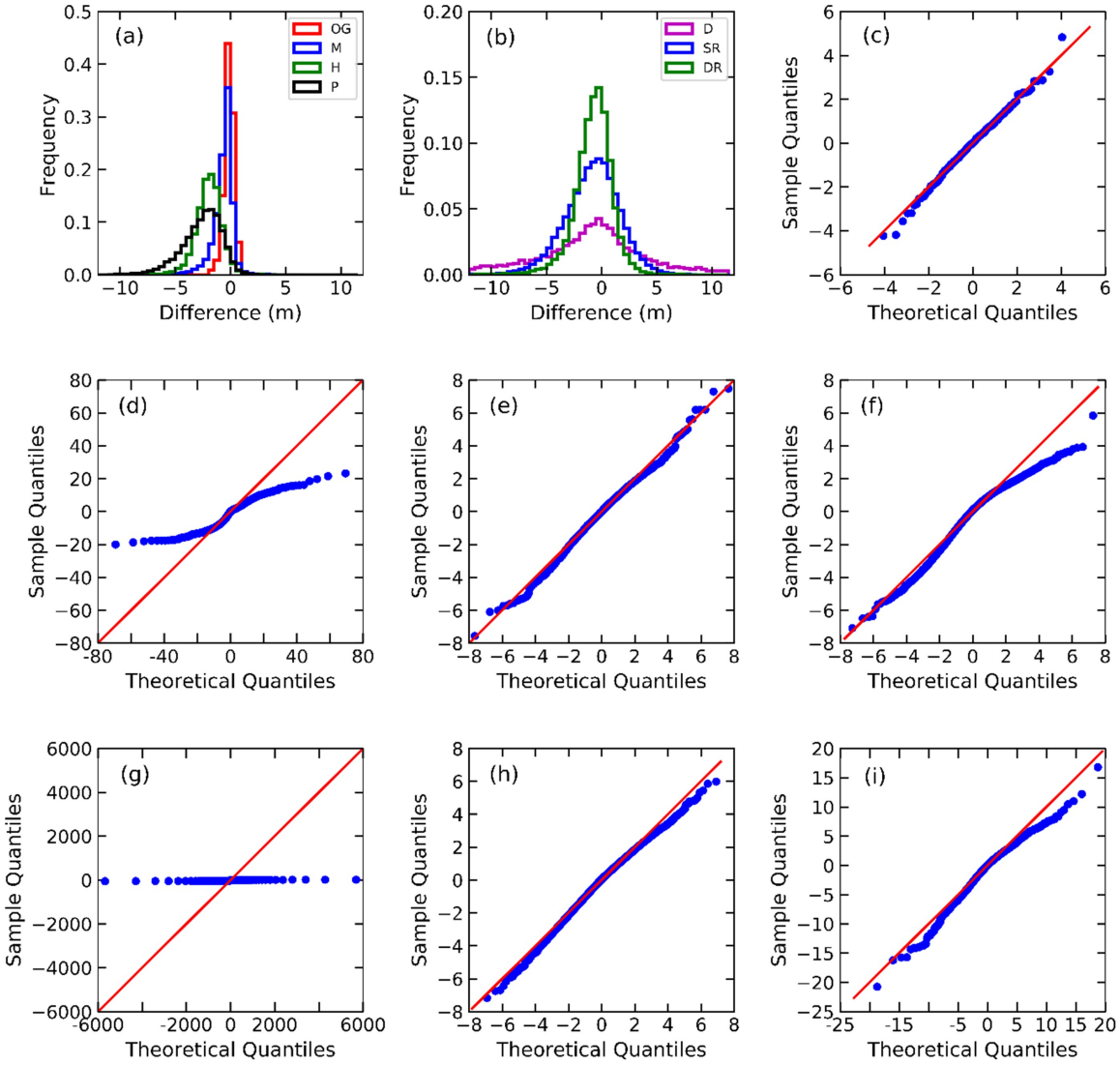

Figure 7. (**a**) Histogram of elevation differences between TDX DEM and LiDAR DSM in open ground (OG) and mangrove (M), hammock (H), and pine (P) forest areas. (**b**) Histogram of elevation differences between TDX DEM and LiDAR DSM in downtown (D), sparse residential (SR), and dense residential (DR) areas. Q-Q plots for open ground (**c**), mangrove forest (**d**), hammock forest (**e**), and pine forest (**f**), downtown (**g**), sparse residential (**h**), and dense residential (**i**) areas.

3.2.2. Forested Area

A comparison of TDX DEM and LiDAR DSM for the 13.5 km^2 mangrove area showed that the TDX DEM captured the spatial variation of mangrove trees in the study area well (Figure 8a). Tall mangrove forest with heights of 14–16 m prevailed close to the coast, while canopy height decreased landward, reaching about 1 m in the dwarf mangrove communities of the interior forest. This was verified by an *R*-squared value of 0.95 for the linear regression equation between LiDAR DSM and TDX DEM elevations (Figure 8c). The value of MNB indicated that TDX DEM underestimated canopy heights by an average of 21% (Table 1). The RMSE and LE90 values of TDX DEM were about 1.15 m and 1.75 m, which reduced slightly to 1.10 m and 1.69 m, respectively, after the removal of pixels with large height errors and height inconsistency. The reason for the small change of *R*-squared values was that the number of pixels with large height errors and height inconsistency was small, representing only 1.4% of the total number of pixels (Table 1).

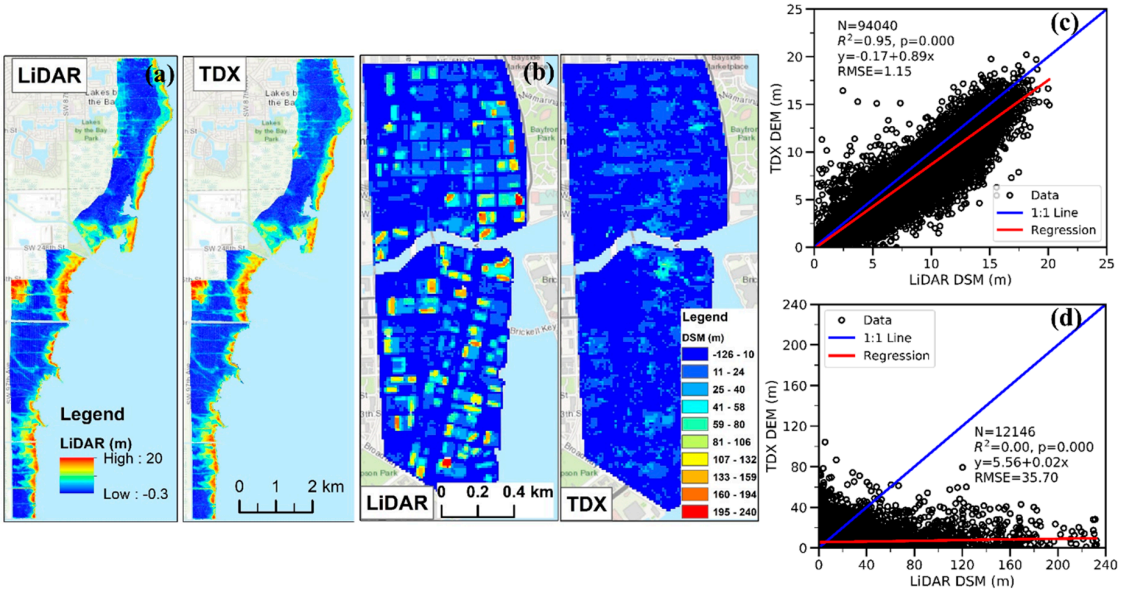

Figure 8. (**a**) LiDAR DSM and TDX DEM for the mangrove forest area along the east coast of South Florida. (**b**) LiDAR DSM and TDX DEM for downtown. Note that the TDX DEM represents the change of mangroves well, while the TDX DEM does not capture many high-rise buildings present in the LiDAR DSM. Linear regression between LiDAR DSM and TDX DEM elevations for the mangrove (**c**) and downtown (**d**) areas.

The protected pine rockland ecosystem in the Everglades National Park (Figure 1), which occurs only in south Florida and the Bahamas, has many species of rare plants. These open stands of slash pine, with a rich understory of herbs and low shrubs, form the matrix in which small tropical hardwood stands are scattered [43]. The TDX DEM elevations for the 1.1 km^2 area occupied by hardwood hammocks exhibited a strong linear relationship with LiDAR DSM elevations (Figure 9), with an *R*-squared value of 0.86 (Table 1). The TDX DEM elevations underestimated the LiDAR tree canopy heights somewhat, generating an MNB value of -23%. The RMSE and LE90 values of TDX DEM without the removal of the large height error or height-inconsistent pixels were about 2.28 m and 3.37 m, respectively, while the removal of such pixels did not change the RMSE value because the number of pixels with large errors was small. In contrast to the good correlation observed between TDX DEM and LiDAR DSM in hardwood hammock, the correlation between these data in 6.1 km^2 pine forest was poor, generating *R*-squared values of 0.14–0.16 (Table 1). The RMSE values with and without the removal of large height error and height-inconsistent pixels were 3.08 m and 3.16 m, respectively. The MNB value of −46% indicated that the TDX DEM elevations largely underestimated the canopy heights of the pine forest. Underestimation of canopy heights increased as the canopy became taller

(Figure 9) because the size of the radar beam from the sensor was larger than the small, thin crowns of tall pine trees, capturing instead the height of mixed tall pine trees and low understory vegetation.

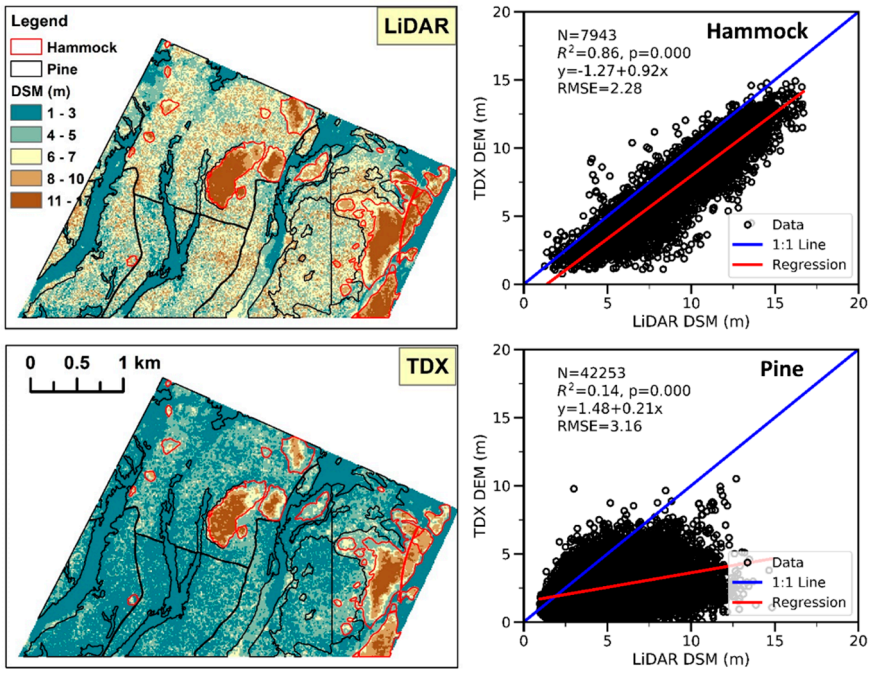

Figure 9. LiDAR DSM and TDX DEM of hardwood hammock and pine forests in Everglades National Park and linear regressions between LiDAR DSM and TDX DEM elevations.

3.2.3. Built Area

A comparison of TDX DEM and LiDAR DSM for the 1.7 km^2 downtown area indicated that the TDX DEM significantly underestimated the heights of tall buildings (Figure 8b,d). The largest building height from TDX DEM was about 110 m, while many pixels from LiDAR DSM exceeded 110 m elevation, with the largest values ranging from 200–240 m. The number of TDX DEM pixels with values less than LiDAR DSM values exceeded the number of TDX DEM pixels with larger values (Figure 8d). TDX DEM and LiDAR DSM pixels with heights less than 40 m were not strongly correlated, and almost no viable TDX DEM measurements were above 80 m (Figure 8d). Over the entire data range, linear regression analysis showed that the *R*-squared value between TDX DEM and LiDAR DSM elevations was less than 0.01 (Table 1). The RMSE and LE90 values were 35.70 m and 51.67 m, respectively (Table 1), much larger than the RMSE for the open ground and forested areas. The RMSE and LE90 values were reduced to 26.86 m and 33.73 m when pixels with height errors larger than 1 m were removed, while the RMSE and LE90 values were reduced to 26.33 m and 29.10 m after removal of large height-inconsistent pixels by selecting the pixels with COM values of 2, 8, and 10. The RMSE and LE90 values were further reduced to 23.48 m and 22.49 m if both criteria were used to select the pixels, but were still worse than the range specified for TDX DEMs. Note that the number of pixels with large height errors and height inconsistency were much larger than in other types of land cover, reaching about half of the total number of pixels (Table 1).

There are two distinct types of residential housing areas in urban Miami: one is a sparse residential area where parcel sizes of residential buildings are large, and trees and lawns occupy the spaces between houses. In this landscape, the vegetated area is usually larger than the built area, and the dense tree canopy overhangs the roads from both sides (Figure 10a). In the second type of residential area, housing is dense, there are fewer open spaces and trees between buildings, and trees covering the roads are not as dense as in the sparse residential area (Figure 10c). Two sample areas, representing sparse and dense residential areas of 11.5 and 15.7 km^2, respectively, were selected to examine the

relationship between TDX DEM and LiDAR DSM. In both cases, more TDX DEM pixels underestimated the elevations of LiDAR DEM pixels than overestimated them (Figure 10b,d).

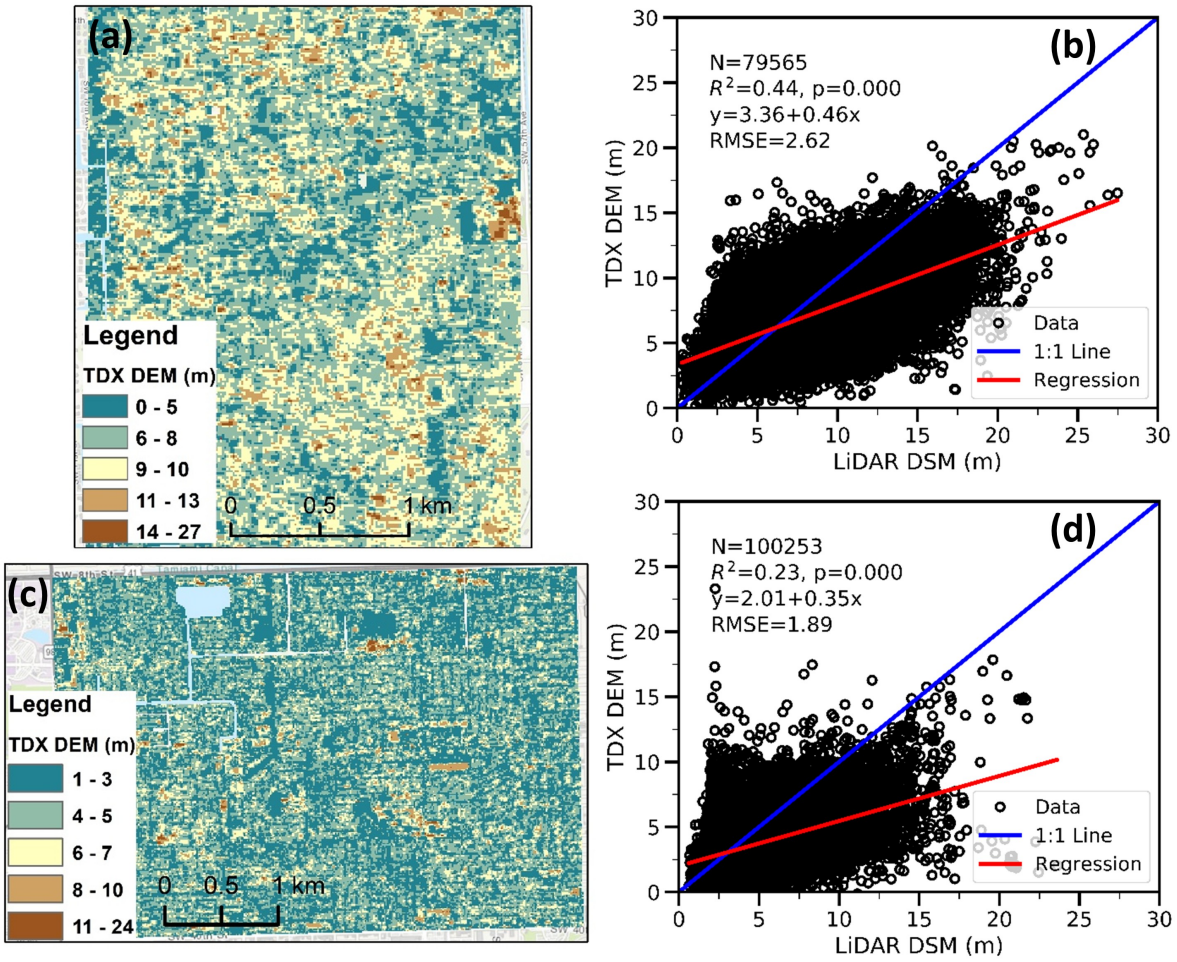

Figure 10. (**a**) TDX DEM for a sparse residential area, (**b**) scatter plot of LiDAR DSM and TDX DEM elevations for the sparse residential area, (**c**) TDX DEM for a dense residential area, and (**d**) scatter plot of LiDAR DSM and TDX DEM elevations for the dense residential area.

TDX DEM and LiDAR DSM elevations in the sparse residential area were reasonably well correlated, with an *R*-squared value of 0.44, while the correlation in the dense residential area was poor, with an *R*-squared value of 0.23 (Table 1). The RMSE values for the sparse and dense residential areas were 2.62 m and 1.89 m, respectively. The removal of pixels of large height errors or height inconsistency did not change RMSE and LE90 values much (Table 1). The MNB values of −2% and −9% for the sparse and dense residential areas, respectively, indicated that the TDX DEM elevations underestimated the LiDAR DSM elevations slightly for both types. The statistical differences in the relationship between TDX DEM and LiDAR DSM elevations for sparse and dense residential areas implied that the composition of buildings, trees, and open ground, including uncovered roads and lawns, might have an effect on the correlation between elevations derived by TDX and LiDAR.

3.2.4. Error Measures

A series of statistical parameters (Equations (1)–(8)) were employed to quantify the errors of TDX DEM. The SD and NMAD values should be similar when the difference between TDX DEM and LiDAR DSM follows a normal distribution because NMAD is the estimator of SD [39,42]. For example, the SD and NMAD values for open ground were 0.46 m and 0.41 m, respectively, and the difference values distributed almost normally in the Q-Q plot (Figure 7c). The ME of open ground was also close to

the median value of the elevation differences. Small differences of 0.15 m and 0.17 m between SD and NMAD also occurred in the hardwood hammock forest and sparse residential areas, respectively, where the Q-Q plot was almost identical to 1:1 line (Figure 7e,h). The fits of the Q-Q plots for differences in the mangrove, pine rockland, and dense residential areas (Figure 7d,f,i) were intermediate between these best cases and the downtown area. The differences between SD and NMAD were 20–28 m (Table 1) in downtown, depending on the criteria for removal of error pixels based on the height errors and consistency codes. The Q-Q plot line for downtown was almost horizontal (Figure 7g). The NMAD values for downtown was much smaller than SD values, indicating that there were many outliers among the elevation difference values. Overall, the changes of the median and NMAD values were less than the variation of ME and SD values across all sample sites. This demonstrated that the median of elevation differences and NMAD were more robust error measures than ME and SD, which supported conclusions from a previous study of DEM accuracy analysis [39].

4. Discussion

The error measures of four cases were calculated for the entire land area of Miami-Dade County and various types of land cover (Table 1). The improvement of accuracy achieved by removing pixels with large height errors and inconsistent heights based on auxiliary data layers accompanying a TDX DEM raster is noteworthy. This can be useful for applications such as deviation of ground pixels by filtering TDX DEM [44] and comparing TDX with SRTM DEMS to document the elevation difference in which missing pixels are acceptable. However, for applications in which the missing pixels of DEMs are not acceptable, the removal of the low-quality pixels may cause a problem. In these cases, one could replace the low-quality pixels by interpolation or by simply keeping the low quality pixels. Fortunately, the amount of low-quality pixels are not high, about 2.5% for the entire study area, with varying amounts for open ground, forest, and built areas discussed below.

4.1. Open Ground

On open ground, the TDX DEM elevations are in very good agreement with LiDAR DSM elevations (Figure 6). The TDX DEMs deliver much more accurate estimates of ground elevation within the study area than the 10 m absolute error range defined by TDX DEM accuracy specification [13]. The LE90 value of 0.79 m is slightly better than the LE90 error of 0.88 m derived by comparing TDX DEM with ICESat measurements in generic cells not covered by ice or forest [12]. Additionally, based on the spatial correlation analysis between TDX DEM and LiDAR DSM profiles (Figure 5), there is no horizontal shift of TDX DEM. Therefore, the TDX DEM provides reliable topographic data source for modeling of geomorphic and hydrologic processes in developing countries, where high resolution DEM data are lacking [45].

However, for flood mapping and analysis of geomorphic modification by human activity in residential areas, the algorithm to separate ground and non-ground measurements from TDX DEM [44] and to create DTM must be developed. The high quality of measurement for open ground delivered by TDX DEM provides reliable seed points to gradually search for additional ground measurements. Unfortunately, the separation of the ground and non-ground elevations is limited by the 12 m resolution of TDX DEM. In heavily built metropolitan areas, where street widths are not significantly larger than the spatial resolution of TDX DEM, the mixing of different objects in a TDX DEM pixel, in combination with shadow effects, prevent consistent ground measurements. Deriving DTM in densely vegetated areas such as mangroves and hardwood hammocks is also difficult because the X-band radar wave (wavelength of 3.1 cm) cannot penetrate through the trees and reach the ground. In semi-developed and sparse or patchy vegetated areas, ground and non-ground features are generally separable in TDX DEM [46,47], and it is in such landscapes that TDX DEM can provide a more reliable DTM for mapping flood impacts.

4.2. Forested Area

TDX DEM has been used extensively to derive digital canopy models (DCM) for estimation of tree height and above ground biomass in urban and natural environments ([23,47–49]. The TDX DEM elevations of the mangrove forest on the southeast Florida coast exhibit the strongest correlation with LiDAR DSM elevations among all forested samples, generating an *R*-squared value of 0.95 (Table 1) which is comparable to previous studies. Feliciano et al. [50] demonstrated that the TDX DCM heights for mangrove forest along the west coast of South Florida had a strong correlation (R^2=0.85) with LiDAR DCM heights based on comparison of the mean heights of the 100 tallest trees in 1-ha plots from LiDAR and TDX data. In our east coast sample area, the RMSE value between TDX DEM and LiDAR DSM elevations was about 1.15 m, less than the RMSE value of 1.89 m in the Feliciano et al. [50] study. This difference may be due to the difference in methods for DCM comparison and the high density of mangrove trees in our sample area, which contrasts with the mangrove forest of the southwest Florida coast, where trees, rivers, and water bodies interweave, resulting in a more complicated DCM. It is notable that the TDX DEM elevations of the mangrove forest underestimate the LiDAR DSM according to the ME and median of difference values (Table 1), and the regression result (Figure 8c). This is expected because the large side-looking angle of 30°–50° of TDX SAR sensors and short X-band radar waves result in penetration of the wave into the vegetation canopy [14,23]. The scattering processes occur mostly in the small branches and foliage of the crown layer [1]. The MNB value of −21% for the TDX DEM mangrove elevations indicates that the scatter center of X-band wave is located at approximately 79% of the LiDAR DSM heights. The true scatter center of the X-band wave should be somewhat lower than 79% of true canopy height, because the LiDAR DSM also provides a slight underestimate of canopy height [51]. The underestimation of canopy heights by TDX DEM is not confined to mangrove forests, but also occurs in many other types of forest, including tropical peat swamp, patchy savanna, boreal, and urban forests [21,23–25]. Both Balzter et al. [21] and Sadeghi et al. [24] demonstrated that the TDX DEM elevations were located between the LiDAR DTM and DSM elevations in patchy savanna and boreal forests.

To derive the DCM of the forest, the ground elevations have to be removed from TDX DEM elevations, thus a DTM is needed for its generation. The DTM can come from LiDAR surveys, stereo analysis of overlapped aerial photographs or high-resolution satellite imagery, and digital topographic maps [47,48,51]. These DTM data already exist for many developed countries but are often not available in developing nations. In the case of the mangrove forest, the DTM elevations can be approximated by mean sea level elevations [52] because the mangrove typically grows in an intertidal zone with near flat topography. However, forests with such level topography are rare on the Earth's surface, and DTMs are needed in mountainous areas with dramatic topographic changes, including boreal forest and hilly urban areas [47,49]. Instead of relying upon an existing DTM, one alternative is to develop methods for extracting ground measurements from TDX DEM data directly, and generate a DTM by interpolating among identified ground pixels [47]. However, the filtering methods are only effective in forests with sparse trees or in patchily forested areas, because TDX DEM pixels representing the ground elevations inside the forest are required to produce a reliable DTM by interpolation.

The TDX DEM elevations of the hardwood hammock forest also show a good correlation with LiDAR DSM elevations, generating an *R*-squared value of 0.86. The MNB value of −23% for the TDX DEM elevations of the hammock indicates that the scatter center of the X-band wave is located at approximately 77% of the LiDAR DSM heights. Although the RMSE value of TDX DEM elevations for hammock is larger than for mangrove, a systematic offset of TDX DEM from LiDAR DSM is obvious in Figure 9, as indicated by a regression line that is almost parallel to the 1:1 line. The reason for the good correlation between TDX DEM and LiDAR DSM elevations is that hardwood hammock consists of a dense stand of broad leaved-trees, resulting in a consistent measurements of tree heights by even scattering of the X-band wave.

The canopy of densely vegetated mangrove and hardwood hammock causes less penetration of X-band radar waves. By contrast, the pine forest forms an open canopy with widely spaced slash pines

and an understory stratum with a mixture of grasses, herbs, palms, and small broadleaved shrubs. The heights of pine trees are typically greater than 9 m, understory shrubs occupy a layer of 0.5–2 m above the ground, and open ground and herbaceous plants range in height from 0–0.5 m [53]. The multiple scattering of radar waves that occurs in these different strata causes an increase in SAR measurement uncertainty [12]. The MNB value of −46% indicates that the X-band wave scatter center is located at about half of adult pine tree heights.

4.3. Built Area

The TDX DEM has also been used to estimate building footprints and heights in urban settings [26]. In the developed areas of South Florida, the TDX DEM elevations showed a large discrepancy from LiDAR DSM in the downtown areas occupied by high-rise buildings, while the discrepancies were much smaller in both sparse and dense residential areas. Other than a few outliers, most TDX DEM elevations were below 10 m in the dense residential area (Figure 10), while a considerable number of TDX DEM elevations for tall trees were higher than 10 m in the sparse residential area (Figure 10). The presence of more trees and open ground in sparse residential areas increases the chance of an X-band wave reaching and scattering back from the tree crown and open ground, resulting in a larger range of DEM elevation values, a stronger correlation between TDX DEM and LiDAR DSM, and a larger RMSE.

The interaction between X-band radar waves with buildings is a complicated process. The side-looking SAR sensor can generate a layover when the foreslope angle of an object exceeds the incident angle of the radar beam and a shadow when the region is not illuminated by SAR [1]. The layover leads to the return waves from objects at different heights imaged into the same pixel, causing ambiguity of elevation measurements, while the shadow results in the absence of data for pixels in the shadow zone. Layover and shadow always occur when a slant incident radar beam meets buildings with vertical walls [46]. According to Rossi and Gernhardt [46], the generation of TDX DEM from SAR measurements involves phase to height conversion and the translation (geocoding) of slant-angle coordinates to geographic coordinates. When illuminated by X-band waves with slant angles of 30°–50°, tall buildings in particular can cause underestimation or failure to capture object heights in the layover zone, and an absence of measurements for objects in the shadow zone. The accuracy of building measurements from the TDX DEM are influenced by the SAR incident angle, the geocoding accuracy, and the sizes, heights, and orientations of buildings [46]. Layover and shadow effects were most notable in downtown areas where high-rise buildings intermingle with narrow streets, causing poor correlations between TDX DEM elevations and LiDAR DSM elevations, as well as the highest percentage of low-quality pixels and largest RMSE values among the landscape types we examined (Table 1 and Figure 8d). Unfortunately, the auxiliary layover and shadow mask layer of TDX DEM provides little information on the locations of layover and shadow pixels in the downtown area. The greatest number of layover and shadow mask pixels in the LSM layer were located inside water bodies in this study, therefore the layover and shadow mask layer were not used in the error analysis.

5. Conclusions

The accuracy of TDX DEM were analyzed against high quality LiDAR DSM for the land area in a coastal urban setting, with a range of land cover types, including open ground, subtropical and tropical forests, high-rise buildings, and single or multi-family residential homes. The results showed that the RMSE and LE90 values of TDX DEM for the entire study area were 2.25 m and 2.30 m. The RMSE and LE90 values of TDX DEM versus LiDAR DSM for open ground were 0.49 m and 0.79 m, respectively. These errors were much smaller than the absolute error of 10 m (at the 90% quantile) specified by the TDX DEM mission statement. It was also demonstrated for the first time that no horizontal shift occurred in TDX DEMs using spatial correlation analysis. Therefore, the global coverage of TDX DEM makes it an essential data layer for studies of geomorphic and hydrologic processes in low relief areas where high-resolution LiDAR data are not available.

The TDX DEM represented the change of canopy heights in the densely vegetated mangrove and hardwood hammock areas reasonably, although the TDX DEM elevations underestimated total tree heights by 21–23% on average. The scattering centers of X-band radar waves in the mangrove and hardwood hammock were located in the top fourth of the canopy, which is occupied by small branches and foliage of tree crowns. The TDX DEM delivered a reliable data source for mapping tree heights in hardwood hammock and mangrove ecosystems where the topography is nearly flat and ground elevations are close to mean sea level. By contrast, the TDX DEM did not represent tree heights well in the pine forest because the multiple scatterings of radar waves from tall pine trees to low shrubs and herbaceous ground surface were imaged into the same pixel.

The correlation between TDX DEM and LiDAR DSM for the built areas was relatively low, with *R*-squared values of 0.44, 0.23, and 0.00 for sparse residential, dense residential, and downtown areas, due to the complex interaction of the incident radar wave with the buildings, trees, and ground. In downtown areas, the layover and shadow effects due to high-rise buildings caused large RMSE and LE90 values of 35.70 m and 51.67 m, respectively, for the differences between TDX DEM and LiDAR DSM elevations, much larger than the error specified for the data. The RMSE/LE90 values of 2.62/4.29 m and 1.89/2.90 m, respectively, for the sparse and dense residential areas were much smaller than the RMSE/LE90 values for downtown.

The values of NMAD were similar to standard deviation values when the differences between TDX DEM and LiDAR DSM elevations followed a normal distribution, as was the case in open ground and hardwood hammock areas. By contrast, NMAD differed remarkably from the standard deviation when the differences did not follow a normal distribution, as was the case in high-rise downtown area. Median and NMAD showed less fluctuation than the mean error and standard deviation across all sample areas with various land cover types, and therefore represented more robust measures of error when comparing TDX DEM to LiDAR DSM elevations.

Since TDX DEM is the first product covering the entire Earth's Surface completely with the highest horizontal and vertical accuracy, it is expected that the dataset will be used extensively in hydrologic, geomorphic, ecologic related applications, particularly in developing countries where higher quality of DEMs are lacking. Although this study found that the vertical accuracy of TDX DEM deteriorated from open ground to forested and built areas by comparing TDX and LiDAR DEMs for a variety of land cover over a large, low-relief coastal urban area, studies involving high-relief terrains and more land cover types are needed in the future to verify and expand the current error ranges to provide guidance for appropriate usage of TDX DEMs. Notably, further horizontal accuracy analyses should be conducted to verify the result from this paper although finding large objects with distinct geometric shapes free from the influence of multiple scattering, shadow, and layover from TDX DEMs is difficult. Additionally, the filtering method to separate ground and non-ground measurements in TDX DEMs and its effectiveness on various land cover types deserve a further study to improve the digital terrain, canopy, and building models in urban and forested areas.

Author Contributions: K.Z. developed the idea and methodology for accuracy analysis by comparing TDX DEMs with LiDAR DEMs; D.G. generated land cover and land use map; K.Z. and D.G. analyzed the data; all co-authors discussed the results, wrote, and edited the manuscript.

Funding: This research was funded by the Office of U.S. Foreign Disaster Assistance, Bureau for Democracy, Conflict and Humanitarian Assistance, U.S. Agency for International Development, under the terms of Participating Agency Program Agreement: AID-OFDA-T-17-00002.

Acknowledgments: This work was supported by "Development of an Integrated Coastal Inundation Forecast Demonstration System in the Caribbean Region—Pilot Project for the Dominican Republic and Haiti" sponsored by the U.S. Agency for International Development (USAID) and National Oceanic and Atmospheric Administration (NOAA). The TanDEM-X DEM tile for Miami-Dade County was provided by the German Aerospace Center through the project "Developing Hurricane Storm Surge Planning and Forecasting Capabilities for Haiti and the Dominican Republic Using TanDEM-X DEMs" (Proposal ID: DEM_HYDR0550)." We thank the Department of Emergency Management of Miami-Dade County for providing the LiDAR data, and City of Miami Beach for providing GPS benchmark measurements, and Dr. Cody Fritz of National Hurricane Center for reviewing the

manuscript. The opinions expressed in this paper are those of authors and do not necessarily reflect views of USAID and NOAA.

Conflicts of Interest: The authors declare no conflict of interest.

References

1. Jensen, J.R. *Remote Sensing of the Environment: An Earth Resource Perspective*, 2nd ed.; Pearson Education: Upper Saddle River, NJ, USA, 2009.
2. Jensen, J.R.; Cowen, D.C. Remote sensing of urban/suburban infrastructure and socio-economic attributes. *Photogramm. Eng. Remote Sens.* **1999**, *65*, 611–622.
3. Krieger, G.; Moreira, A.; Fiedler, H.; Hajnsek, I.; Werner, M.; Younis, M.; Zink, M. TanDEM-X: A satellite formation for high-resolution SAR interferometry. *IEEE Trans. Geosci. Remote Sens.* **2007**, *45*, 3317–3341. [CrossRef]
4. Shan, J.; Toth, C.K. *Topographic Laser Ranging and Scanning: Principles and Processing*; CRC Press: Boca Raton, FL, USA, 2018; ISBN 9781498772273.
5. Woodhouse, I.H. *Introduction to Microwave Remote Sensing*; CRC Press: Boca Raton, FL, USA, 2005.
6. Farr, T.G.; Rosen, P.A.; Caro, E.; Crippen, R.; Duren, R.; Hensley, S.; Kobrick, M.; Paller, M.; Rodriguez, E.; Roth, L. The shuttle radar topography mission. *Rev. Geophys.* **2007**, *45*. [CrossRef]
7. Yan, K.; Di Baldassarre, G.; Solomatine, D.P.; Schumann, G.J. A review of low-cost space-borne data for flood modelling: Topography, flood extent and water level. *Hydrol. Process.* **2015**, *29*, 3368–3387. [CrossRef]
8. Li, Z.; Zhu, Q.; Gold, C. *Digital Terrain Modeling: Principles and Methodology*; CRC Press: Boca Raton, FL, USA, 2005; ISBN 9780415324625.
9. Rodriguez, E.; Morris, C.S.; Belz, J.E. A global assessment of the SRTM performance. *Photogramm. Eng. Remote Sens.* **2006**, *72*, 249–260. [CrossRef]
10. Falorni, G.; Teles, V.; Vivoni, E.R.; Bras, R.L.; Amaratunga, K.S. Analysis and characterization of the vertical accuracy of digital elevation models from the Shuttle Radar Topography Mission. *J. Geophys. Res. Earth Surf.* **2005**, *110*, F02005. [CrossRef]
11. Sanders, B.F. Evaluation of on-line DEMs for flood inundation modeling. *Adv. Water Resour.* **2007**, *30*, 1831–1843. [CrossRef]
12. Rizzoli, P.; Martone, M.; Gonzalez, C.; Wecklich, C.; Tridon, D.B.; Bräutigam, B.; Bachmann, M.; Schulze, D.; Fritz, T.; Huber, M. Generation and performance assessment of the global TanDEM-X digital elevation model. *ISPRS J. Photogramm. Remote Sens.* **2017**, *132*, 119–139. [CrossRef]
13. Wessel, B. *TanDEM-X Ground Segment–DEM Products Specification Document*; German Space Center: Cologne, Germany, 2016.
14. Zink, M.; Bachmann, M.; Brautigam, B.; Fritz, T.; Hajnsek, I.; Moreira, A.; Wessel, B.; Krieger, G. TanDEM-X: The new global DEM takes shape. *IEEE Geosci. Remote Sens. Mag.* **2014**, *2*, 8–23. [CrossRef]
15. Huber, M.; Wessel, B.; Kosmann, D.; Felbier, A.; Schwieger, V.; Habermeyer, M.; Wendleder, A.; Roth, A. Ensuring globally the TanDEM-X height accuracy: Analysis of the reference data sets ICESat, SRTM and KGPS-Tracks. In Proceedings of the 2009 IEEE International Conference on Geoscience and Remote Sensing, Cape Town, South Africa, 12–17 July 2009; Volume 2, pp. 769–772.
16. Wessel, B.; Gruber, A.; Huber, M.; Breunig, M.; Wagenbrenner, S.; Wendleder, A.; Roth, A. Validation of the absolute height accuracy of TanDEM-X DEM for moderate terrain. In Proceedings of the 2014 IEEE Geoscience and Remote Sensing Symposium, Quebec City, QC, Canada, 13–18 July 2014; pp. 3394–3397.
17. Wessel, B.; Huber, M.; Wohlfart, C.; Marschalk, U.; Kosmann, D.; Roth, A. Accuracy assessment of the global TanDEM-X digital elevation model with GPS data. *ISPRS J. Photogramm. Remote Sens.* **2018**, *139*, 171–182. [CrossRef]
18. Soergel, U.; Jacobsen, K.; Schack, L. The TanDEM-X Mission: Data collection and deliverables. In *Photogrammetric Week*; Institute for Photogrammetry: Stuttgart, Germany, 2013; pp. 193–203. Available online: http://www.ifp.uni-stuttgart.de/publications/phowo13/170Soergel.pdf (accessed on 27 January 2019).
19. Hajnsek, I.; Busche, T.; Krieger, G.; Zink, M.; Schulze, D.; Moreira, A. *TanDEM-X Ground Segment Announcement of Opportunity: TanDEM-X Science Phase*; TD-PD-PL-0032; German Aerospace Center, Microwaves and Radar Institute: Weßling, Germany, 2014.

20. Baade, J.; Schmullius, C. TanDEM-X IDEM precision and accuracy assessment based on a large assembly of differential GNSS measurements in Kruger National Park, South Africa. *ISPRS J. Photogramm. Remote Sens.* **2016**, *119*, 496–508. [CrossRef]
21. Balzter, H.; Baade, J.; Rogers, K. Validation of the TanDEM-X Intermediate digital elevation model with airborne LiDAR and differential GNSS in Kruger National Park. *IEEE Geosci. Remote Sens. Lett.* **2016**, *13*, 277–281. [CrossRef]
22. Feng, L.; Muller, J.P. ICESat validation of TanDEM-X I-DEMS over the UK. *ISPRS-International Arch. Photogramm. Remote Sens. Spat. Inf. Sci.* **2016**, *XLI-B4*, 129–136. [CrossRef]
23. Schlund, M.; von Poncet, F.; Kuntz, S.; Boehm, H.-D.V.; Hoekman, D.H.; Schmullius, C. TanDEM-X elevation model data for canopy height and aboveground biomass retrieval in a tropical peat swamp forest. *Int. J. Remote Sens.* **2016**, *37*, 5021–5044. [CrossRef]
24. Sadeghi, Y.; St-Onge, B.; Leblon, B.; Simard, M. Canopy height model (CHM) derived from a TanDEM-X InSAR DSM and an airborne lidar DTM in boreal forest. *IEEE J. Sel. Top. Appl. Earth Obs. Remote Sens.* **2016**, *9*, 381–397. [CrossRef]
25. Schreyer, J.; Lakes, T. Deriving and evaluating city-wide vegetation heights from a TanDEM-X DEM. *Remote Sens.* **2016**, *8*, 940. [CrossRef]
26. Marconcini, M.; Marmanis, D.; Esch, T.; Felbier, A. A novel method for building height estmation using TanDEM-X data. In Proceedings of the 2014 IEEE International Geoscience and Remote Sensing Symposium (IGARSS), Quebec City, QC, Canada, 13–18 July 2014; pp. 4804–4807.
27. Hajnsek, I.; Busche, T.; Schulze, D.; Buckreub, S.; Moreira, A. *TanDEM-X: TanDEM-X Digital Elevation Models Announcement of Opportunity*; TD-PD-AO-0033; German Aerospace Center, Microwaves and Radar Institute: Weßling, Germany, 2016.
28. Renken, R.A.; Dixon, J.; Koehmstedt, J.; Ishman, S.; Lietz, A.C.; Marella, R.L.; Telis, P.; Rodgers, J.; Memberg, S. *Impact of Anthropogenic Development on Coastal Ground-Water Hydrology in Southeastern Florida, 1900–2000*; USGS: Reston, VA, USA, 2005; Volume 1.
29. Zhang, K. Analysis of non-linear inundation from sea-level rise using LIDAR data: A case study for South Florida. *Clim. Chang.* **2011**, *106*, 537–565. [CrossRef]
30. Gruber, A.; Wessel, B.; Huber, M.; Roth, A. Operational TanDEM-X DEM calibration and first validation results. *ISPRS J. Photogramm. Remote Sens.* **2012**, *73*, 924–2716. [CrossRef]
31. Gruber, A.; Wessel, B.; Martone, M.; Roth, A. The TanDEM-X DEM mosaicking: Fusion of multiple acquisitions using InSAR quality parameters. *IEEE J. Sel. Top. Appl. Earth Obs. Remote Sens.* **2016**, *9*, 1047–1057. [CrossRef]
32. America, A.C. *Surveyor and Mapper Report for the 2015 Aerial LiDAR Specific Purpose Survey of Miami-Dade County*; Aerial Cartographics of America: Orlando, FL, USA, 2015. Available online: https://coast.noaa.gov/htdata/lidar2_z/geoid12b/data/5038/supplemental/fl2015_miami_dade_m5038_lidar_report.pdf (accessed on 27 January 2019).
33. SFWMD. *2009 SFWMD Photointeperation Key*; SFWMD: West Palm Beach, FL, USA, 2011.
34. Welch, R.; Madden, M.; Doren, R.F. Mapping the Everglades. *Photogramm. Eng. Remote Sens.* **1999**, *65*, 163–170.
35. Hochmair, H.H.; Gann, D.; Benjamin, A.; Fu, Z. *Miami-Dade County Urban Tree Canopy Assessment*; GIS Center, Florida International University: Miami, FL, USA, 2016.
36. FDOT. *Florida Land Use and Cover and Forms Classification System: Handbook*, 3rd ed.; Thematic Mapping Section: Tallahassee, FL, USA, 1999.
37. Wendleder, A.; Wessel, B.; Roth, A.; Breunig, M.; Martin, K.; Wagenbrenner, S. TanDEM-X Water Indication Mask: Generation and First Evaluation Results. *IEEE J. Sel. Top. Appl. Earth Obs. Remote Sens.* **2013**, *6*, 171–179. [CrossRef]
38. Davis, J. *Statistics and Data Analysis In Geology*, 3rd ed.; John Willey & Sons, Inc.: New York, NY, USA, 2002; ISBN 978-0-471-17275-8.
39. Höhle, J.; Höhle, M. Accuracy assessment of digital elevation models by means of robust statistical methods. *ISPRS J. Photogramm. Remote Sens.* **2009**, *64*, 398–406. [CrossRef]
40. Müller, J.; Gärtner-Roer, I.; Thee, P.; Ginzler, C. Accuracy assessment of airborne photogrammetrically derived high-resolution digital elevation models in a high mountain environment. *ISPRS J. Photogramm. Remote Sens.* **2014**, *98*, 58–69. [CrossRef]

41. Hampel, F.R. The influence curve and its role in robust estimation. *J. Am. Stat. Assoc.* **1974**, *69*, 383–393. [CrossRef]
42. Leys, C.; Ley, C.; Klein, O.; Bernard, P.; Licata, L. Detecting outliers: Do not use standard deviation around the mean, use absolute deviation around the median. *J. Exp. Soc. Psychol.* **2013**, *49*, 764–766. [CrossRef]
43. Ross, M.S.; O'Brien, J.J.; Ford, R.G.; Zhang, K.; Morkill, A. Disturbance and the rising tide: The challenge of biodiversity management on low-island ecosystems. *Front. Ecol. Environ.* **2009**, *7*, 471–478. [CrossRef]
44. Geiß, C.; Wurm, M.; Breunig, M.; Felbier, A.; Taubenböck, H. Normalization of TanDEM-X DSM data in urban environments with morphological filters. *IEEE Trans. Geosci. Remote Sens.* **2015**, *53*, 4348–4362. [CrossRef]
45. Gutenson, J.L.; Follum, M.L.; Snow, A.D.; Wahl, M.D. Large-scale flood inundation modeling in data sparse environments using TanDEM-X terrain data. *Open Water J.* **2017**, *4*, 4.
46. Rossi, C.; Gernhardt, S. Urban DEM generation, analysis and enhancements using TanDEM-X. *ISPRS J. Photogramm. Remote Sens.* **2013**, *85*, 120–131. [CrossRef]
47. Schreyer, J.; Geiß, C.; Lakes, T. TanDEM-X for large-Area modeling of urban vegetation height: Evidence from Berlin, Germany. *IEEE J. Sel. Top. Appl. Earth Obs. Remote Sens.* **2016**, *9*, 1876–1887. [CrossRef]
48. Lagomasino, D.; Fatoyinbo, T.; Lee, S.; Feliciano, E.; Trettin, C.; Simard, M. A comparison of mangrove canopy height using multiple independent measurements from land, air, and space. *Remote Sens.* **2016**, *8*, 327. [CrossRef]
49. Sadeghi, Y.; St-Onge, B.; Leblon, B.; Prieur, J.-F.; Simard, M. Mapping boreal forest biomass from a SRTM and TanDEM-X based on canopy height model and Landsat spectral indices. *Int. J. Appl. Earth Obs. Geoinf.* **2018**, *68*, 202–213. [CrossRef]
50. Feliciano, E.A.; Wdowinski, S.; Potts, M.D.; Lee, S.-K.; Fatoyinbo, T.E. Estimating Mangrove Canopy Height and Above-Ground Biomass in the Everglades National Park with Airborne LiDAR and TanDEM-X Data. *Remote Sens.* **2017**, *9*, 702. [CrossRef]
51. Zhang, K.; Thapa, B.; Ross, M.; Gann, D. Remote sensing of seasonal changes and disturbances in mangrove forest: A case study from South Florida. *Ecosphere* **2016**, *7*, 1–23. [CrossRef]
52. Simard, M.; Zhang, K.; Rivera-Monroy, V.H.; Ross, M.S.; Ruiz, P.L.; Castañeda-Moya, E.; Twilley, R.R.; Rodriguez, E. Mapping height and biomass of mangrove forests in Everglades National Park with SRTM elevation data. *Photogramm. Eng. Remote Sens.* **2006**, *72*, 299–311. [CrossRef]
53. Houle, P.; Zhang, K.; Ross, M.; Simard, M. Use of airborne lidar for the assessment of landscape structure in the pine forests of Everglades national park. In Proceedings of the 2006 IEEE International Conference on Geoscience and Remote Sensing, Denver, CO, USA, 31 July–4 August 2006; pp. 1960–1963.